JOURNAL OF SOLID STATE CHEMISTRY 4, 94–102 (1972)

# Electrochemical Deposition and Dissolution of Tungsten Oxide Bronzes

R. A. FREDLEIN AND A. DAMJANOVIC

*Electrochemistry Laboratory, University of Pennsylvania, Philadelphia, Pennsylvania 19104*

Received May 5, 1971

The potentiostatic deposition of sodium tungsten bronzes from $Na_2WO_4/WO_3$ melts can produce large single crystals. A bronze grown in the same melt constitutes a reliable reference electrode. The current density, current efficiency and composition of the bronze remain constant throughout deposition. Potential against current data permit some mechanistic analysis on the basis of initial charge transfer to a $WO_3$ tetramer. Dissolution is not the simple reverse of deposition and enhanced anodic currents are interpreted as simultaneous bronze dissolution and sodium dissolution from the deposit.

The composition of the bronze is determined solely by the melt composition but {100} faces are favored over {110} faces at lower temperatures. Chemical and X-ray structure analyses of mixed bronzes (bronzes incorporating a second transition metal) are consistent with formulas $Na_xW_{1-y}Z_yO_3$ (Z = Nb, Ta, Zr, V, Co). Failure to grow bronzes incorporating Re is suggested to be due to formation of a Re/W oxide polymer which undergoes preferential charge transfer but which does not deposit.

## I. Introduction

Recently, oxide bronzes, particularly sodium tungsten bronzes, have attracted attention as possible electrocatalysts for oxygen reduction in fuel cells and energy storage devices (*1–5*). Electrocatalysis is known to be greatly affected by impurity metal atoms incorporated into the bronze (*3–5*) and to a lesser extent by crystal face and composition (*4*).

Electrochemical reduction of $Na_2WO_4/WO_3$ melts produce crystals well suited to these studies. However, the usual constant current method of growing bronzes (*6*) takes place with decreasing current density and accompanying changes in electrode potential. Consequently, if two or more potential dependent reactions occur during the growth of a crystal, their rates may vary in different ways during the growth process and produce variations in the composition of the deposit. The constant current deposition of mixed bronzes[1] (crystals in which tungsten is partially replaced by a second transition metal) could, for example, result in an inhomogeneous deposit. Further, the constant current technique of bronze deposition has yielded data of little mechanistic significance. This paper describes bronze growth by potentiostatic deposition, i.e., the polarization of the deposit is maintained constant throughout growth, and its application to the production of mixed bronzes incorporating Nb, Ta, Zr, Co, or V. The data permit some analysis of the mechanisms of deposition and dissolution.

[1] By analogy to other mixed crystals we prefer the term mixed bronze (*4*) to the term doped bronze (*7, 8*) when several percent of the tungsten atoms are replaced. Doped bronze better describes the incorporation of impurities, in unspecified sites, in the ppm range (*3, 4*).

## II. Experimental

### A. Growth of Pure Bronzes

*The cell.* Deposition was carried out under a slow stream (15 ml $min^{-1}$) of purified argon in the cell previously described (*4*). The melt, $Na_2WO_4$ (Baker Analyzed)/$WO_3$ (K and K 99.5%), contacts only high-purity alumina (McDanel) and gold which is very noble in these melts. Other ceramics were found to be readily attacked by the melt, while boron nitride and graphite reduce the melt and form red, bronze-like conducting deposits. Silica was rapidly devitrified by the melt. The temperature of the melt was measured by a Chromel–Alumel thermocouple and controlled to ±3°C (Barber Coleman 427P).

*Procedure.* Two electrodes were lowered into the melt, and a bronze was grown on one by passing a

constant current of 7 mA overnight. This bronze was used as the reference electrode.

Seed crystals of *ca.* 1.5 × 1.5 × 3 mm were cut with a precision diamond wafering machine, parallel to the crystal faces (visual adjustment), from a bronze grown in a melt of the same composition. The seed was attached to the third electrode, lowered into the melt, and a bronze grown by maintaining the seed at a chosen potential negative to that of the reference bronze electrode (Wenking potentiostat). A gold wire served as the counterelectrode (anode). The current was recorded (Moseley 680) and after *ca.* 1000 C had passed, the bronze was removed from the melt and cooled in a stream of argon. The solidified melt around the bronze was removed by washing in boiling dilute sodium hydroxide solution (*ca.* 1 hr).

### *B. Growth of Mixed Bronzes*

These crystals were prepared from $Na_2WO_4/WO_3$ melts containing a second transition metal oxide ($Ta_2O_5$, $Nb_2O_5$, $ZrO_2$, $V_2O_5$, and $Co_2O_3$). A new melt was prepared after the growth of the reference electrode to avoid depleting the melt of the second transition metal oxide. The melt surrounding the bronze was removed by washing in boiling water.

### *C. Kinetics of Deposition and Dissolution*

Before the bronze was removed from the melt steady-state, anodic and cathodic *I–V* curves were obtained both by increasing and decreasing the electrode potential. No significant dissolution or growth of bronzes occurred during these experiments.

### *D. Structure Examination*

X-Ray diffraction angles and relative intensities of diffracted beams were determined on powdered samples; scan rate, 0.125 deg/min (Norelco Diffractometer; Ni-filtered Cu$K\alpha$ radiation).

### *E. Composition Determination*

The sodium composition of pure bronzes was computed from the lattice constant using the relation (*9*)

$$a_0 = 0.0820x + 3.7845 \text{ (Å)} \qquad (1)$$

where $a_0$ is the lattice constant, and $x$ is the subscript in $Na_xWO_3$. For mixed bronzes and some pure bronzes, sodium was determined by atomic absorption at 590 nm (Perkin–Elmer 303). Powdered bronze was fused with 100 times its weight of ammonium persulfate in Vycor tubes and the solidified melt dissolved in hot 0.35 *M* *d*-tartaric acid. Standard sodium chloride solutions contained an appropriate amount of $WO_3$ which was dissolved in the same way as bronzes themselves. Table I compares the analytical results for some pure bronzes.

TABLE I

SODIUM COMPOSITION[a] OF SODIUM TUNGSTEN BRONZES DETERMINED BY BOTH X-RAY DIFFRACTION AND CHEMICAL ANALYSIS

| Crystal No. | Chem. analysis | X-Ray diffraction |
|---|---|---|
| 13 | 0.69 | 0.70 |
| 18 | 0.63 | 0.62 |

[a] Composition of the bronze is given by $x$ in $Na_xWO_3$.

Niobium, tantalum,[2] zirconium,[2] and tungsten[2] were determined colorimetrically. A powdered bronze was fused with 50 times its weight of potassium bisulfate and the solidified melt dissolved in 0.35 *M* *d*-tartaric acid. Tungsten interferes with the determination of niobium as the thiocyanate complex (*10*) and, therefore, standard solutions were prepared to contain the same amount of tungsten as the bronze being examined. Oxygen composition was calculated by difference.

Gold was not detected in the emission spectra of powdered samples (*11*) (limit of detection *ca.* 10 ppm).

## III. Results

### *A. Sodium Tungsten Bronze Crystals*

The conditions of growth of the crystals and the results are summarized in Table II. Bronzes grown in a melt of 40 mole % $WO_3$ were of cubic habit ({100} faces), while those grown in a melt of 49 mole % $WO_3$ were dodecahedral ({110} faces). Cubic and dodecahedral bronzes as large as 1 cm in linear dimensions were easily grown.[3] Attempts to grow a crystal of high sodium content ($x > 0.9$) at temperatures exceeding 750°C produced only a deposit of tungsten (*12*), but a well-formed yellow bronze with {100} faces was grown at 725°C.

The composition of pure sodium tungsten bronzes is, within the narrow range of temperature and potential studied, dependent only on the composition of the melt (Table II). Lower temperatures favor the formation of bronzes with cubic faces rather than those of the dodecahedral faces. Thus, a bronze crystal grown at the same potential in the melt of 46 mole % $WO_3$ grows with the cubic faces (crystal

[2] Analyses made by Coleman Laboratories, Philadelphia, PA.

[3] Photographs are shown in Ref. (4).

TABLE II

RESULTS OF EXPERIMENTS ON THE POTENTIOSTATIC GROWTH OF SODIUM TUNGSTEN BRONZE CRYSTALS

| Crystal No. | Temp (°C) | $-\eta^a$ (mV) | Melt composition (mole % $WO_3$) | Composition $x$ in $Na_xWO_3$ | Crystal faces formed | Deposit form | Yield (%) |
|---|---|---|---|---|---|---|---|
| 13 | 803 | 30 | 40 | 0.70[b] | {100} | single | 91 |
| 14 | 803 | 40 | 40 | 0.73 | {100} | single | 95 |
| 15 | 803 | 60 | 40 | 0.73 | {100} | multi | 100 |
| 16 | 803 | 30 | 40 | 0.72 | {100} | single | 99 |
| 18 | 803 | 40 | 49 | 0.62 | {110} | single | 83 |
| 19 | 803 | 50 | 49 | — | {110} | single | — |
| 20 | 803 | 55 | 49 | 0.62 | {110} | single | 88 |
| 21 | 803 | 75 | 49 | 0.63 | —[d] | multi | — |
| 22 | 803 | 30 | 49 | 0.61 | {110} | single | — |
| 23 | 803 | 40 | 49 | 0.64 | {110} | multi | 87 |
| 24 | 803 | 65 | 49 | 0.63 | —[d] | multi | — |
| 25 | 803 | 50 | 46 | 0.66 | {110} | multi | 89 |
| 27 | 750 | 50 | 46 | 0.67 | {100} | multi | 103 |
| 28 | 750 | 34 | 49 | 0.61 | {110} | single | 91 |
| 29 | 750 | 30 | 46 | 0.65 | {100} | single | 91 |
| 30 | 725 | 30 | 10 | 0.93 | {100} | single | — |
| 31 | 800 | —[e] | 60 | 0.35[c] | — | multi | — |
| 32 | 800 | —[e] | 55 | 0.43[c] | — | multi | — |

[a] $\eta$ is the potential of the growing crystal with respect to the bronze reference electrode.
[b] Determined from lattice constant.
[c] Determined from atomic absorption analysis.
[d] These crystals were needles with either {100} or {110} faces.
[e] Bronze grown at constant current.

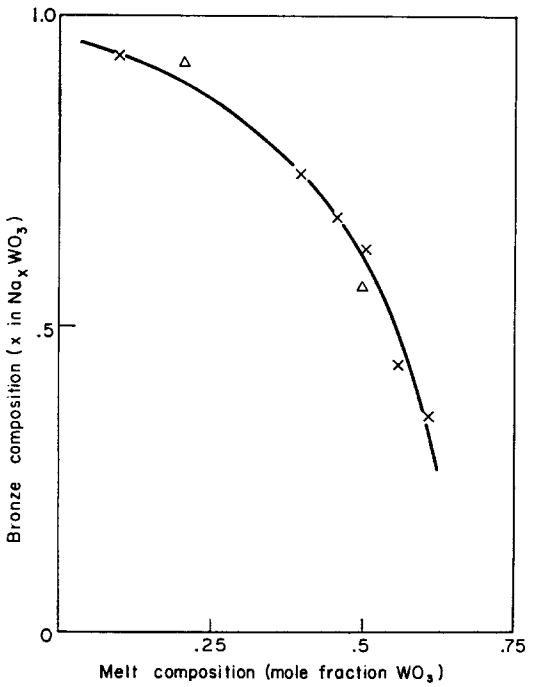


FIG. 1. Bronze composition ($x$ in $Na_xWO_3$) against melt composition.

29) at 750°C but with the dodecahedral faces (crystal 25) at 803°C and the composition is unchanged (Table II).

In some cases, {100} and {110} faces were obtained outside their normal range of $x$ values by growth over a crystal of lower or higher $x$ value, respectively. Figure 1 is a plot of bronze composition against composition of the melt and includes the data of Vest *et al.* (*13*). A smooth relation exists between bronze composition and melt composition up to about 50 mole % $WO_3$. Beyond about 55 mole % $WO_3$, the curve is possibly discontinuous due to a change of crystal structure of the bronze.

All crystals, except 31 and 32, were confirmed by X-ray diffraction analysis to be of primitive cubic lattice. Crystals 31 and 32 were of mixed tetragonal and cubic phases and their composition was determined by chemical analysis.

### *B. Growth of Mixed Bronzes*

The conditions of growth of these crystals and the results are summarized in Table III. Attempts to grow crystals of high niobium or tantalum content at 800°C from melts containing 5% $Nb_2O_5$ or 1% $Ta_2O_5$ resulted in blue-grey deposits with little

TABLE III

RESULTS OF EXPERIMENTS ON THE GROWTH OF MIXED BRONZES

| Crystal No. | Temp (°C) | Melt composition $WO_3$ (mole %) | Melt composition Additive (mole %) | Bronze composition[a] | $a_0$ obsd (Å) | $a_0$ calcd[b] (Å) |
|---|---|---|---|---|---|---|
| 36 | 803 | 40 | 0.50 $Nb_2O_5$ | $Na_{0.70}W_{0.94}Nb_{0.06}O_3$[c] | 3.8447 | 3.8419 |
| 37 | 803 | 40 | 1.0 | $Na_{0.76}W_{0.84}Nb_{0.16}O_3$[c] | 3.8475 | 3.8468 |
| 38 | 800 | 40 | 0.30 $Ta_2O_5$ | $Na_{0.70}W_{0.88}Ta_{0.12}O_{3.0}$ | 3.8457 | 3.8419 |
| 51 | 750 | 40 | 0.30 | $Na_{0.74}W_{0.90}Ta_{0.10}O_{3.3}$ | 3.8461 | 3.8452 |
| 48 | 750 | 40 | 0.42 | $Na_{0.72}W_{0.93}Ta_{0.07}O_{3.2}$ | 3.8466 | 3.8435 |
| 52 | 750 | 40 | 0.30 | $Na_{0.69}W_{0.93}Ta_{0.07}O_{3.3}$ | 3.8418 | 3.8411 |
| 39 | 800 | 40 | 0.18 | $Na_{0.71}W_{0.94}Ta_{0.06}O_{3.0}$ | 3.8432 | 3.8427 |
| 50 | 750 | 40 | 0.24 | $Na_{0.74}W_{0.96}Ta_{0.04}O_{3.2}$ | 3.8436 | 3.8452 |
| 49 | 750 | 40 | 0.06 | $Na_{0.68}W_{0.97}Ta_{0.03}O_{3.0}$ | 3.8423 | 3.8403 |
| 42 | 800 | 49 | 0.30 | $Na_{0.62}W_{0.94}Ta_{0.06}O_{3.2}$ | 3.8468 | 3.8353 |
| 54 | 800 | 40 | 2.0 $ZrO_2$ | $Na_{0.68}W_{0.98}Zr_{0.02}O_{3.1}$ | 3.8430 | 3.8403 |
| 43 | 800 | 40 | 1.0 | $Na_{0.69}W_{0.99}Zr_{0.01}O_{3.1}$ | 3.8421 | 3.8411 |
| 44 | 800 | 40 | 1.0 | — | — | — |
| 45 | 800 | 40 | 0.90 $Co_2O_3$ | — | — | — |
| 46 | 800 | 40 | 0.90 | — | — | — |
| 47[d] | 750 | 40 | 0.15 $V_2O_5$ | — | — | — |

[a] Oxygen by difference.
[b] Calculated from the sodium composition assuming Eq. (1) is valid for mixed bronzes.
[c] Tungsten analysis not performed; the total transition metal content assumed to be 1 and that of oxygen 3.
[d] Grown at −60 mV with respect to bronze reference electrode. All others grown at −35 to −40 mV.

metallic luster and high resistivity at room temperature. Vanadium bronze could only be grown at high overpotentials (−60 mV) in melts containing ⩽0.15 mole % $V_2O_5$. At lower overpotentials, it appears that a rapid dissolution of the bronze occurs. Addition of as little as 0.1% $ReO_3$ or $Re_2O_7$ to $Na_2WO_4/WO_3$ melt completely inhibited the deposition of bronze even after a sufficient number of coulombs to reduce all rhenium in the melt to the metal had been passed. After more current was passed traces of a metallic deposit were observed.

The mixed bronzes are darker in color than pure sodium tungsten bronzes grown in melts of the same tungstic oxide content. The bronze of highest tantalum content was similar to that with highest niobium content in that it had a distinct blue tint. All the mixed bronzes listed in Table III, with the exception of crystal 42, had well-formed cubic morphology. Crystal 42, a low sodium bronze containing tantalum, exhibited both {100} and {110} faces.

Bronzes containing Ta, Nb, and Zr have primitive cubic lattice. The lattice constants are listed in Table III. The square roots of the peak intensities of the reflections relative to that from the (200) plane are compared in Table IV for a pure sodium tungsten bronze and bronzes of nearly the same sodium content containing Nb, Ta, or Zr.

TABLE IV

X-RAY DIFFRACTION INTENSITY DATA FOR SODIUM TUNGSTEN BRONZES AND MIXED BRONZES

| Crystal No. | 13 | 36 | 37 | 39 | 48 | 54 |
|---|---|---|---|---|---|---|
| Crystal plane | $I^{1/2}$[a] | $I^{1/2}$ | $I^{1/2}$ | $I^{1/2}$ | $I^{1/2}$ | $I^{1/2}$ |
| 100 | 2.0 | 2.03 | 1.61 | 1.95 | 2.36 | 1.90 |
| 110 | 1.45 | 1.75 | 1.12 | 1.65 | 1.24 | 1.24 |
| 111 | 0.543 | 0.654 | 0.404 | 0.539 | 0.457 | 0.527 |
| 200 | 1.00 | 1.00 | 1.00 | 1.00 | 1.00 | 1.00 |
| 210 | 1.07 | 1.22 | 0.790 | 1.02 | 0.931 | 0.841 |
| 211 | 0.976 | 1.03 | 0.680 | 0.966 | 0.663 | 0.727 |
| 220 | 0.606 | 0.767 | 0.379 | 0.585 | 0.473 | 0.479 |
| 221, 300 | 0.673 | 0.981 | 0.530 | 0.834 | 0.640 | 0.606 |
| 310 | 0.603 | 0.886 | 0.474 | 0.558 | 0.480 | 0.464 |
| 311 | 0.398 | 0.654 | 0.316 | 0.467 | 0.414 | — |
| 222 | 0.354 | 0.401 | — | 0.381 | 0.192 | — |
| 320 | 0.399 | 0.500 | 0.344 | 0.394 | 0.345 | — |
| 321 | 0.515 | 0.732 | 0.468 | 0.846 | 0.448 | 0.505 |

[a] $I$ is the intensity of the reflection from a given plane relative to that from the (200) plane.

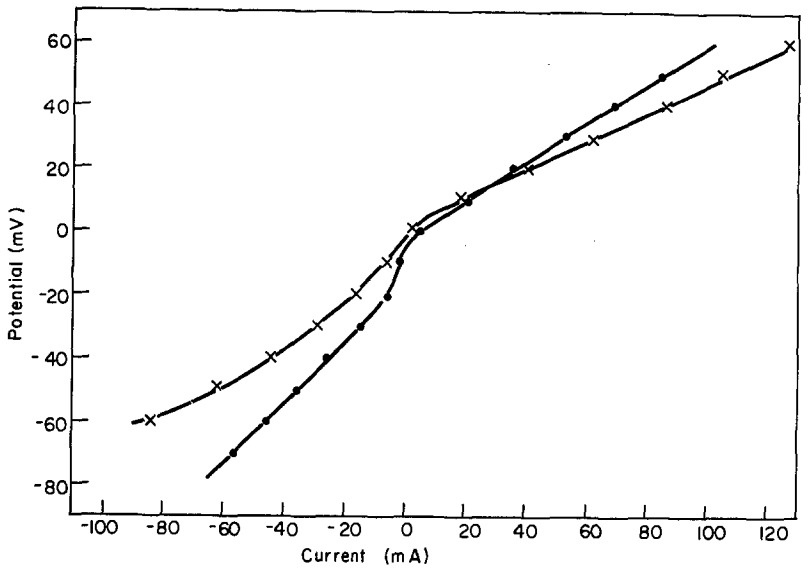


FIG. 2. *I–V* Curves for dissolution and deposition of bronzes.
× = crystal 14, $Na_{0.73}WO_3$
● = crystal 22, $Na_{0.61}WO_3$

### C. Potential–Current Density Relationship

The curves of current against potential for electrochemical dissolution and deposition of bronzes are shown in Fig. 2 for a crystal with cubic faces and one with dodecahedral faces. Anodic lines are linear from low overpotentials, but the cathodic lines are curved at low overpotentials and only at higher overpotentials tend to become linear. The deviation from the linearity is more pronounced for high sodium content bronzes with {100} faces, than for low sodium content bronzes with {110} faces. Bronzes of the intermediate sodium content show intermediate behavior regardless of morphology.

## IV. Discussion

### A. Mode of Growth of Bronzes

At a constant electrode potential the total deposition current $I$ on a bronze with cubic faces and volume $v$ is given by

$$I = 6iv^{2/3}, \tag{2}$$

where $i$ is the current density for a given potential and melt composition. The rate of growth of the bronze is given by

$$dv/dt = 6\epsilon Miv^{2/3}/xFd, \tag{3}$$

where $M$ is the molecular weight of $Na_xWO_3$, $x$ the sodium composition, $\epsilon$ the current efficiency ($0.85 < \epsilon < 1.0$) (Table II), $d$ the density of the bronze and $F$ the Faraday equivalent. Integrating Eq. (3) for the initial condition $v = v_0$, the volume of the seed crystal, yields

$$v^{1/3} = (2\epsilon Mit/xdF) + v_0^{1/3}. \tag{4}$$

Substituting Eq. (2) into Eq. (4), one obtains

$$I^{1/2} = (4.90\epsilon Mi^{3/2}t/xFd) + 2.45\, i^{1/2} v_0^{1/3}. \tag{5}$$

The densities of the bronzes at melt temperature are unknown but the slopes of the $I^{1/2}$ against $t$ plots (Fig. 3) agree with the values predicted from Eq. (5) when the density is taken as .75 times that calculated from the room temperature lattice constant (Table V). The linearity of the plots shows that $i$, $\epsilon$ and $x$[4] remain constant during the deposition and further that a bronze constitutes a reliable reference electrode in these melts.

### B. Mechanism of Bronze Deposition

The rates of deposition and dissolution are potential dependent and hence are not controlled by diffusion or chemical processes occurring in the melt. Banks et al. (*14*) have shown that deposition is accompanied by charge transfer to a $WO_3$ tetramer and present evidence that $Na(WO_3)_4$ is the deposited

[4] The constancy of $x$ within the deposit does not imply that the sodium composition was constant during the growth process, as fast equilibration of sodium at high temperatures could occur.

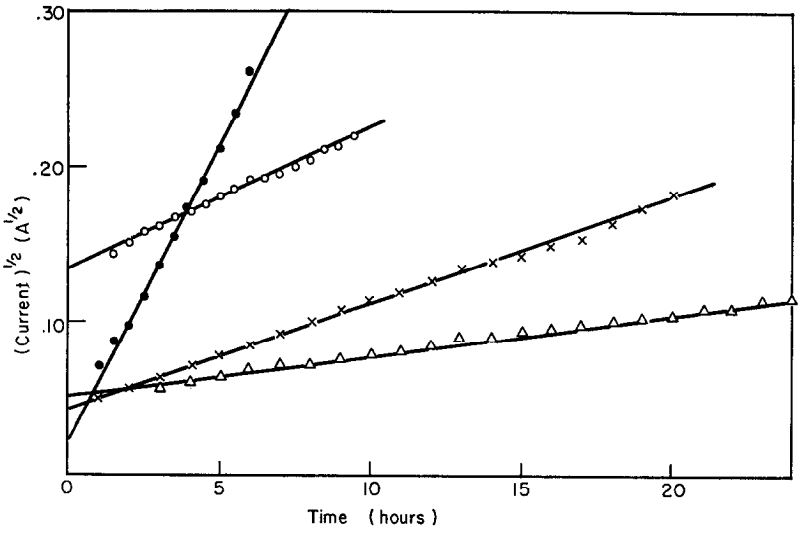


FIG. 3. $I^{1/2}$ against time for deposition of bronzes.

o = crystal 14, $Na_{0.73}WO_3$

× = crystal 20, $Na_{0.62}WO_3$

● = crystal 24, $Na_{0.63}WO_3$

△ = crystal 28, $Na_{0.61}WO_3$

TABLE V

CALCULATED AND OBSERVED SLOPES OF $I^{1/2a}$ AGAINST TIME PLOTS FOR THE DEPOSITION OF SODIUM TUNGSTEN BRONZES

| Crystal No. | Obsd slope ($A^{1/2}$ $sec^{-1}$) | Calcd slope[b] ($A^{1/2}$ $sec^{-1}$) |
|---|---|---|
| 14 | $2.5 \times 10^{-6}$ | $2.5 \times 10^{-6}$ |
| 20 | $1.9 \times 10^{-6}$ | $2.0 \times 10^{-6}$ |
| 24 | $1.1 \times 10^{-5}$ | —[c] |
| 28 | $7.6 \times 10^{-7}$ | $7.1 \times 10^{-7}$ |

[a] $I$ is the deposition current.

[b] Density taken as 0.75 times the room temperature density.

[c] This crystal had dendritic type of growth and the area was not calculated.

species under conditions equivalent to those of the present work:

$$\underset{(a)}{(WO_3)_4} + e^- \leftrightarrows \underset{(b)}{(WO_3)_4^-} \qquad (6)$$

$$\underset{(b)}{(WO_3)_4^-} + Na^+ \leftrightarrows \underset{(c)}{[Na(WO_3)_4]_{ad}}. \qquad (7)$$

Two paths may be envisaged by which a bronze of composition $x = 0.6 - 0.8$ can be formed from the adspecies $[Na(WO_3)_4]_{ad}$. Path I involves subsequent sodium discharge. One example of such a mechanism is (Path I):

$$\underset{(c)}{[Na(WO_3)_4]_{ad}} \leftrightarrows 4\underset{(d)}{[Na_{0.25}WO_3]_{lattice}} \qquad (8)$$

$$\left(\frac{4}{4x-1}\right)\underset{(d)}{[Na_{0.25}WO_3]_{lattice}} + Na^+ + e^- \leftrightarrows \left(\frac{4}{4x-1}\right)\underset{(e)}{[Na_xWO_3]_{lattice}}. \qquad (9)$$

Path II involves loss of $WO_3$, either directly from the lattice of a low sodium bronze (*15*) or from the adspecies prior to incorporation in the lattice as shown (Path II):

$$\underset{(c)}{[Na(WO_3)_4]_{ad}} \rightleftarrows \frac{1}{x}\underset{(f)}{[Na_xWO_3]_{ad}} + \left(\frac{4x-1}{x}\right)WO_3 \qquad (10)$$

$$\underset{(f)}{[Na_xWO_3]_{ad}} \leftrightarrows \underset{(g)}{[Na_xWO_3]_{lattice}}. \qquad (11)$$

Path II is analogous to metal deposition from aqueous solution in which the adspecies progressively loses molecules from the solvation shell (*16*).

The kinetics of growth and dissolution can be conveniently analyzed making use of the relation (*17*)

$$i = -i_0\{\exp(-\eta F/\nu RT)(\beta n + \overleftarrow{\gamma}) - \exp(\eta F/\nu RT)[(1-\beta)n + \vec{\gamma}]\}, \quad (12)$$

where $i$ is the net current density (positive for dissolution and negative for deposition) at overpotential $\eta$, $i_0$ the exchange current density, $\beta$ the symmetry factor, $\nu$ the stoichiometric number of the rate determining step (r.d.s.), $n$ the total number of electrons transferred in the r.d.s., $\overleftarrow{\gamma}$ and $\vec{\gamma}$ the total number of electrons transferred before and after the r.d.s.

$$\eta = V - V_R, \quad (13)$$

where $V$ is the electrode potential and $V_R$ the reversible potential. The rate expressions for the various paths and rate determining steps are listed in Table VI.

Both the expressions $(\alpha^{(2x+1/2)} - \alpha^{-(2x-1/2)})$ and $(\alpha - 1)$, where $\alpha = \exp(-\eta F/RT)$ and $x$ is the sodium composition of the bronze, are linear against deposition and dissolution current (Figs. 4 and 5). The expression $(\alpha^{1/2} - \alpha^{-1/2})$ is linear against dissolution current only, while the other rate expressions (Table VI) do not give linear relations.

The linear relations of Figs. 4 and 5 suggest that deposition of the bronzes could take place via path I with I(de) as the r.d.s. or via path II with II(bc), (cf), or (fg) as the r.d.s. Both plots, however, exhibit a sudden increase of slope (3–4 times) close to $\eta = 0$ on the anodic side. It is not possible to explain this change of slope by an increase of $i_0$. If II(fg) is the r.d.s., then

$$i_0 = xFk_{fg}[Na_xWO_3]_{ad,R}\,\theta_{Na_xWO_3},$$

where $[Na_xWO_3]_{ad,R}$ is the surface concentration of the adspecies at $\eta = 0$ and $\theta_{Na_xWO_3}$ is the concentration of growth sites suitable for incorporation of adspecies with an average composition $Na_xWO_3$ into the lattice. Hence a change of $i_0$ implies a change of $\theta_{Na_xWO_3}$ and a 3–4 fold increase in this quantity is improbable in a narrow potential span of *ca.* 10 mV. Similar arguments apply to steps I(de), II(bc) and (cf). This reasoning also precludes a change from one r.d.s. to another within a specific path. A plausible explanation is to be found in terms of sodium dissolution from the bronze.[5] Thermodynamically the bronzes may be regarded as a solution of sodium in a $WO_3$ matrix (*18*) and potentials anodic to the reversible bronze deposition–dissolution potential constitute an overpotential for sodium dissolution as well as bronze dissolution. For rate determining charge transfer the sodium dissolution current is given by

$$i = i_0^*(\alpha^{1/2} - \alpha^{-1/2})$$

TABLE VI

RATE EXPRESSIONS FOR THE DEPOSITION AND DISSOLUTION OF SODIUM TUNGSTEN BRONZES BY VARIOUS MECHANISMS

| Path | Rate determining step | Rate expression[a] |
|---|---|---|
| I | (ab) | $-i_0(\alpha^{1/2} - \alpha^{-(4x-1/2)})$ |
| I | (bc), (cd) | $-i_0(\alpha - \alpha^{-(4x-1)})$ |
| I | (de) | $-i_0(\alpha^{(2x+1/2)} - \alpha^{-(2x-1/2)})$ |
| II | (ab) | $-i_0(\alpha^{1/2} - \alpha^{-1/2})$ |
| II | (bc), (cf), (fg) | $-i_0(\alpha - 1)$ |

[a] $\alpha = \exp(-\eta F/RT)$, $x$ is the sodium composition of the bronze ($x$ in $Na_xWO_3$) and $\beta$ taken as 1/2.

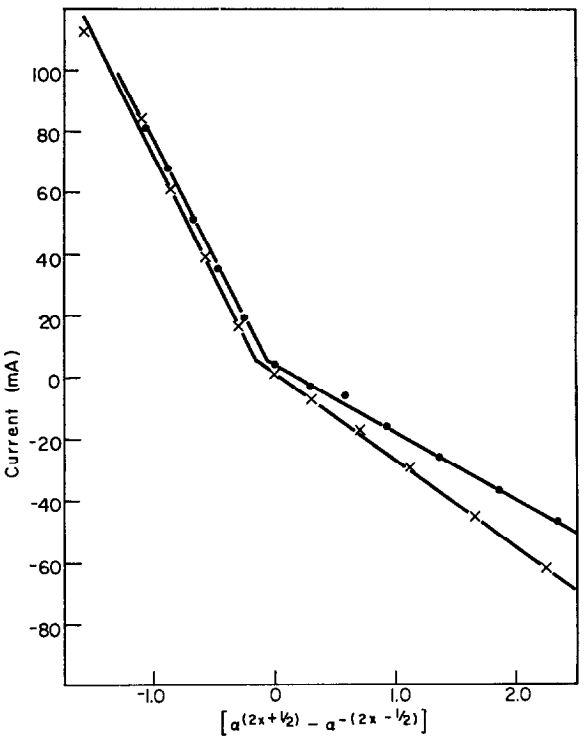


FIG. 4. Deposition and dissolution current against $(\alpha^{(2x+1/2)} - \alpha^{-(2x-1/2)})$.

× = crystal 14, $Na_{0.73}WO_3$
● = crystal 22, $Na_{0.61}WO_3$
$\alpha = \exp(-\eta F/RT)$

[5] The anodic dissolution of sodium from bronzes has been shown to occur in aqueous solution at room temperature (*4*).

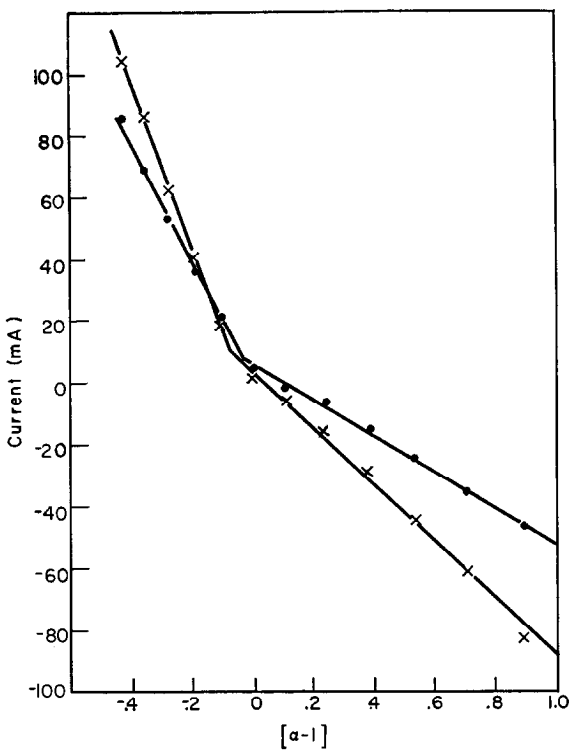


FIG. 5. Deposition and dissolution current against $(\alpha - 1)$.
× = crystal 14, $Na_{0.73}WO_3$
● = crystal 22, $Na_{0.61}WO_3$
$\alpha = \exp(-\eta F/RT)$

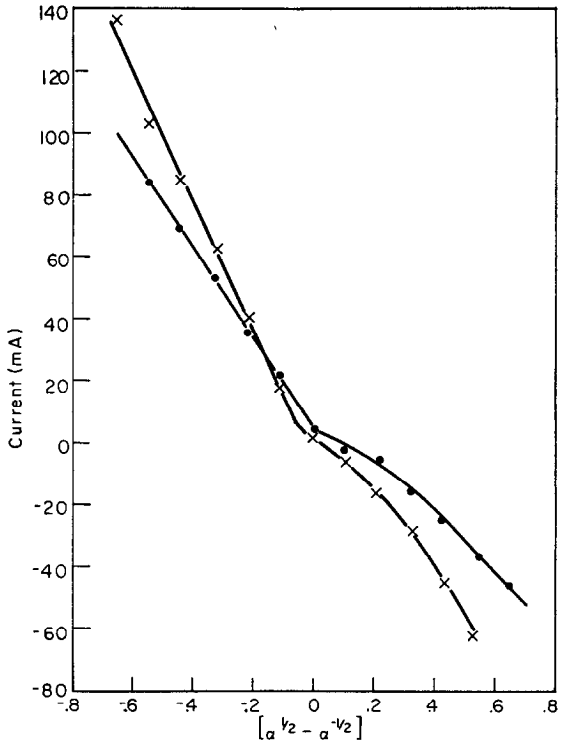


FIG. 6. Deposition and dissolution current against $(\alpha^{1/2} - \alpha^{-1/2})$.
× = crystal 14, $Na_{0.73}WO_3$
● = crystal 22, $Na_{0.61}WO_3$
$\alpha = \exp(-\eta F/RT)$

where $i_0$* is the exchange current density for sodium dissolution. In the range of anodic potentials studied $(\alpha^{1/2} - \alpha^{-1/2})$, $(\alpha - 1)$ and $(\alpha^{(2x+1/2)} - \alpha^{-(2x-1/2)})$ are approximately linearly related and the observed linear anodic lines are to be expected with an enhanced slope.

Provided a change of mechanism does not occur it should be readily possible to distinguish between the two paths by studying the process at higher overpotentials, where $\alpha$ is no longer an approximately linear function of $(\alpha^{(2x+1/2)} - \alpha^{-(2x-1/2)})$. Experiments in the Tafel region, where one of the partial currents can be neglected, should be particularly valuable. Since these crystals were prepared for subsequent electrocatalysis studies, experiments at high overpotentials were avoided to preserve the surface from erosion.

### C. *Mixed Bronzes*

The lattice constants of mixed bronzes are only slightly higher than those calculated, using Eq. (1), for pure bronzes of the same sodium composition (Table III). Weller et al. (7) have found slightly larger lattice expansions but still consistent with incorporation of the second transition metal atoms in tungsten sites.

Table IV compares X-ray intensity data for bronzes with the high Ta, Nb, and Zr contents with those of a pure bronze of the same sodium composition. The data are normalized with respect to the intensity of the reflection from the (200) plane. Consequently, reflections from planes (100), (111), (210), (221), and (300) should be decreased while those from planes (110), (211), (220), and (310) should be little changed, relative to those from a pure bronze, if the second transition metal occupies interstitial sites together with sodium atoms. Similarly, reflections from planes (100), (110), (210), (211), (221), (300), and (310) should be decreased while those from planes (111) and (220) should be little changed if the second transition metal occupies face positions (0, 1/2, 1/2) in the cubic lattice. The data of Table IV show neither

trend and provide evidence that the second transition metal replaces tungsten atoms in the structure.

On this basis, the mixed bronzes may be assigned formulas, $Na_xW_{1-y}Z_yO_3$, where Z is the second transition metal. The oxygen composition, calculated by difference is 3 within experimental error.[6]

It is difficult to explain why the addition of a small amount of a rhenium oxide to the melt completely inhibits bronze deposition even after sufficient current has been passed to reduce all the rhenium to metal. One possibility is that the rhenium oxide is incorporated into a polymer with tungsten oxide and this polymer undergoes preferential charge transfer. If this species does not deposit, no bronze is formed but it can presumably undergo further charge transfer, and vastly more charge would then be required to reduce this polymeric species to metal.

## Acknowledgments

The authors thank Professor J. O'M. Bockris, Messrs. J. McHardy and J. A. Christopulos for valuable discussion. The work was supported by the U.S. Army Electronics Command, Ft. Monmouth, N.J. (Contract No. DAAB07-69-C-0077).

## References

1. D. B. Sepa, A. Damjanovic, and J. O'M. Bockris, *Electrochim. Acta* **12**, 746 (1967).

[6] The oxygen content of pure bronzes deposited electrolytically is slightly greater than 3 (*19*).

2. A. Damjanovic, D. Sepa, and J. O'M. Bockris, *J. Res. Inst. Catal. Hokkaido Univ.* **16**, 1 (1968).
3. J. O'M. Bockris, A. Damjanovic, and J. McHardy, *Proc. Int. Symp. Fuel Cells 3rd Brussels*, 15 (1969).
4. R. A. Fredlein and J. McHardy, *Proc. Power Sources Symp. 24th* 175 (1970).
5. J. H. Fishman, J. F. Henry, and S. Tessore, *Electrochim. Acta* **14**, 1314 (1969).
6. E. Banks and A. Wold, "Preparative Inorganic Reactions" (W. L. Jolly, Ed.), Vol. 4, p. 237, Interscience, New York, 1968.
7. P. F. Weller and B. E. Taylor, *J. Solid State Chem.* **2**, 9 (1970).
8. P. F. Weller, B. E. Taylor, and R. L. Mohler, *Mater. Res. Bull.* **5**, 465 (1970).
9. B. W. Brown and E. Banks, *J. Amer. Chem. Soc.* **76**, 963 (1954).
10. H. Freund and A. E. Levitt, *Anal. Chem.* **23**, 1813 (1951).
11. J. McHardy, personal communication.
12. G. L. Davis and C. H. R. Gentry, *Metallurgia* **53**, 3 (1956).
13. R. W. Vest, M. Griffel, and J. F. Smith, *J. Chem. Phys.* **28**, 293 (1958).
14. E. Banks, C. W. Fleischmann, and L. Meites, *J. Solid State Chem.* **1**, 372 (1970).
15. M. E. Straumanis, *J. Amer. Chem. Soc.* **71**, 679 (1949).
16. J. O'M. Bockris and A. Damjanovic, "Modern Aspects of Electrochemistry" (J. O'M. Bockris and B. E. Conway, Eds.), Vol. 3, p. 224, Butterworths, London, 1964.
17. R. Parsons, *Trans. Faraday Soc.* **47**, 1332 (1951).
18. P. G. Dickens and M. S. Whittingham, *Quart. Rev.* **22**, 30 (1968).
19. J. H. Ingold and R. C. DeVries, *Acta Metall.* **6**, 736 (1958).